Carbon 95 (2015) 239–249

Contents lists available at ScienceDirect

Carbon

journal homepage: www.elsevier.com/locate/carbon

On the intrinsic ripples and negative thermal expansion of graphene

Yangfan Hu [a, *], Jiapeng Chen [b], Biao Wang [a, b, **]

[a] Sino-French Institute of Nuclear Engineering and Technology, Sun Yat-Sen University, 510275 Guangzhou, China
[b] School of Physics and Engineering, Sun Yat-sen University, 510275 Guangzhou, China

ARTICLE INFO

Article history:
Received 29 July 2014
Received in revised form
28 July 2015
Accepted 7 August 2015
Available online 13 August 2015

Keywords:
Ripples
Negative thermal expansion
Soft phonon modes

ABSTRACT

The intrinsic ripples of suspended graphene have attracted intensive attention due to their influence on the electronic transport and other properties. Negative thermal expansion (NTE), another unconventional phenomenon found in graphene, can be utilized to control the intrinsic ripples in a reversible way, thus opening new perspective for application. In this case, understanding the mutual relation and physical origin of the intrinsic ripples and NTE is crucial, especially since they are both widely observed in other 2D materials. Here we clarify through lattice dynamical analysis that at low temperature the two phenomena are both intrinsic for any 2D crystals with a honeycomb structure (or any monatomic 2D crystals). We find that the intrinsic ripples, generally believed to be caused by thermal fluctuation, have another origin that is the appearance of soft ZA modes near long wavelength limit when the lattice constant is shortened. Moreover, the soft ZA modes and NTE have the same physical origin at low temperature. At finite temperature, NTE is dominantly caused by the "vibrational elongation" effect owing to large out-of-plane fluctuation according to our calculation based on self-consistent phonon theory.

1. Introduction

Uncovering the nature of its intrinsic ripples [1,2] is one of the most challenging and vital problems concerning suspended graphene. On one hand, its academic interest derives from the Peierls–Landau–Mermin argument, raised almost 80 years ago, about the non-existence of low-dimensional crystalline state [3–5]. On the other hand, the crumpled morphology of a suspended graphene has a profound impact on its physical properties, including electronic transport [6–12], magnetoresistance [13], mechanical strength [14], electromechanical coupling [15] and chemical activity [16,17]. Currently, the spontaneous appearance of ripples in graphene is attributed to several factors, including thermal fluctuations [18,19], spontaneously and/or thermally generated strains [20] and adsorbed OH molecules sitting on random sites [21]. Despite these existing explanations, we believe that the ripple problem for suspended graphene is still far from settled because of many related yet unsolved issues. To name a few of these issues, the spontaneous ripples found by Meyer et al. [1] in graphene are with a size range of $50-100$ Å, what factor determines this size and is it controllable? Are the ripples randomly distributed or with a stable pattern? Is the rippled state unique for graphene or is it a common feature for any 2D materials?

Another unusual structural property of graphene is that it possesses NTE coefficient [22], which is also found in graphene oxide [23,24]. Actually, before the experiments, the NTE coefficient of graphene has been predicted and explained by using a theoretical method combining first principle calculation and lattice dynamical analysis [25]. Moreover, it is found that NTE can be used to control the intrinsic ripples in a reversible way [20], which is of great merits for exploration of new tunable graphene-based devices. At this stage, it is natural to think that certain internal relation exists between these two types of exotic structural properties of graphene, which has never been truly understood.

In this work, we try to elucidate the relevance between the intrinsic ripples and the NTE in graphene. By doing so, direct answers or clues to the many unsolved issues concerning the intrinsic ripples are obtained, as well as a deeper understanding of the origin of the ripple formation and the NTE coefficient in graphene. The discussion is divided into two parts: one for low temperature condition where the effect of thermal fluctuation is neglected, and the other for finite temperature condition where thermal fluctuation is significant and even compatible with lattice spacing.

* Corresponding author.
** Corresponding author. Sino-French Institute of Nuclear Engineering and Technology,State Key Laboratory of Optoelectronic Materials and Technologies, Sun Yat-sen University, 510275 Guangzhou, China.
E-mail addresses: huyf3@mail.sysu.edu.cn (Y. Hu), wangbiao@mail.sysu.edu.cn (B. Wang).

http://dx.doi.org/10.1016/j.carbon.2015.08.022
0008-6223/

2. Low-temperature analysis

At low temperature, according to the theory of lattice dynamics in the harmonic approximation [26], the phonon frequencies are determined by

$$\omega_{\mathbf{q}n}^2 = \sum_{\alpha,\beta,k,k'} \varepsilon_{\alpha k}(\mathbf{q},n)\varepsilon_{\beta k'}(\mathbf{q},n) D_{\alpha\beta}\begin{pmatrix}\mathbf{q}\\ k,k'\end{pmatrix}, \tag{1}$$

where $\varepsilon_{\alpha k}(\mathbf{q}, n)$ is polarization of the kth atom in the unit cell in the α-axis direction of the nth branch of phonon with wave vector $\mathbf{q}$, and

$$D_{\alpha\beta}\begin{pmatrix}\mathbf{q}\\ k,k'\end{pmatrix} = \frac{1}{m}\sum_{\mathbf{l}'} K_{\alpha\beta}\begin{pmatrix}0,\mathbf{l}'\\ k,k'\end{pmatrix} e^{-i\mathbf{q}\mathbf{l}'_{k'}} \tag{2}$$

is the dynamical matrix. $\mathbf{l}'_{k'}$ is the lattice vector pointing to the unit cell in which atom k' is lying. In Eq. (2)

$$K_{\alpha\beta}\begin{pmatrix}\mathbf{0},\mathbf{l}'\\ kk'\end{pmatrix} = \left(\frac{\partial^2 \mathrm{U}}{\partial u_\alpha\begin{pmatrix}\mathbf{0}\\ k\end{pmatrix}\partial u_\beta\begin{pmatrix}\mathbf{l}'\\ k'\end{pmatrix}}\right)_0, \tag{3}$$

where $\mathrm{U} = \sum \Phi_i$ denotes the total potential energy of the system, and Φ_i is the potential energy possessed by the ith atom. The subscript "0" means that the derivative takes value at equilibrium lattice structure, and $u_\alpha\begin{pmatrix}0\\ k\end{pmatrix}$ denotes the αth component of the displacement vector of the kth atom in the 0th unit cell.

A basic character of the vibrational motion of 2D materials is that the restoring force for the out-of-plane motion is caused by changes of bond angles [27]. This means that an effective description of the interatomic potential in this case has to be a multi-body potential. For example, the carbon–carbon potential LCBOPII [28] describes the nearest neighbor interaction between carbon atoms in graphene as a function of the bond length as well as four related bond angles. Describing the system with LCBOPII, the potential energy possessed by the ith atom Φ_i takes the following form [29,30].

$$\Phi_i = \frac{1}{2}\left[\sum_{j,|\mathbf{r}_{ij}|=a}\varphi_1\left(\mathbf{r}_{ij},\theta_{ijk}\right) + \sum_{j,|\mathbf{r}_{ij}|=\sqrt{3}a}\varphi_2\left(\mathbf{r}_{ij}\right) + \sum_{j,|\mathbf{r}_{ij}|=2a}\varphi_3\left(\mathbf{r}_{ij}\right)\right], \tag{4}$$

where θ_{ijk} denotes the bond angle between neighboring bond $\mathbf{r}_{ij}$ and $\mathbf{r}_{ik}$ $(k \neq i, j)$. $\varphi_1(\mathbf{r}_{ij}, \theta_{ijk})$, $\varphi_2(\mathbf{r}_{ij})$ and $\varphi_3(\mathbf{r}_{ij})$ denote respectively the nearest neighbor interaction, the second nearest neighbor interaction and the third nearest neighbor interaction. Geometrically, $\mathbf{r}_{ij}$ and θ_{ijk} are both function of $u_\alpha\begin{pmatrix}0\\ k\end{pmatrix}$ and $u_\beta\begin{pmatrix}\mathbf{l}'\\ k'\end{pmatrix}$ $(\alpha, \beta = 1, 2, 3)$. Hence for any 2D lattice structure, the following expansion can always be done concerning the second order derivative of the nearest neighbor interaction $\varphi_1(\mathbf{r}_{ij}, \theta_{ijk})$

$$\begin{aligned}\left(\frac{\partial^2\varphi_1\left(\mathbf{r}_{ij},\theta_{ijk}\right)}{\partial u_\alpha\begin{pmatrix}\mathbf{0}\\ k\end{pmatrix}\partial u_\beta\begin{pmatrix}\mathbf{l}'\\ k'\end{pmatrix}}\right)_0 &= \left(\frac{\partial\varphi_1}{\partial r_{ij}}\right)_0\left(\frac{\partial^2 r_{ij}}{\partial u_\alpha\begin{pmatrix}\mathbf{0}\\ k\end{pmatrix}\partial u_\beta\begin{pmatrix}\mathbf{l}'\\ k'\end{pmatrix}}\right)_0 + \sum_{k\neq i,j}\left(\frac{\partial\varphi_1}{\partial\cos\theta_{ijk}}\right)_0\left(\frac{\partial^2\cos\theta_{ijk}}{\partial u_\alpha\begin{pmatrix}\mathbf{0}\\ k\end{pmatrix}\partial u_\beta\begin{pmatrix}\mathbf{l}'\\ k'\end{pmatrix}}\right)_0\\ &+\left(\frac{\partial^2\varphi_1}{\partial r_{ij}^2}\right)_0\left(\frac{\partial r_{ij}}{\partial u_\alpha\begin{pmatrix}\mathbf{0}\\ k\end{pmatrix}}\frac{\partial r_{ij}}{\partial u_\beta\begin{pmatrix}\mathbf{l}'\\ k'\end{pmatrix}}\right)_0 + \sum_{k,l\neq i,j}\left(\frac{\partial^2\varphi_1}{\partial\cos\theta_{ijk}\partial\cos\theta_{ijl}}\right)_0\left(\frac{\partial\cos\theta_{ijk}}{\partial u_\alpha\begin{pmatrix}\mathbf{0}\\ k\end{pmatrix}}\frac{\partial\cos\theta_{ijl}}{\partial u_\beta\begin{pmatrix}\mathbf{l}'\\ k'\end{pmatrix}}\right)_0\\ &+\sum_{k\neq i,j}\left(\frac{\partial^2\varphi_1}{\partial\cos\theta_{ijk}\partial r_{ij}}\right)_0\left[\left(\frac{\partial r_{ij}}{\partial u_\alpha\begin{pmatrix}\mathbf{0}\\ k\end{pmatrix}}\frac{\partial\cos\theta_{ijk}}{\partial u_\beta\begin{pmatrix}\mathbf{l}'\\ k'\end{pmatrix}}\right)_0 + \left(\frac{\partial r_{ij}}{\partial u_\beta\begin{pmatrix}\mathbf{l}'\\ k'\end{pmatrix}}\frac{\partial\cos\theta_{ijk}}{\partial u_\alpha\begin{pmatrix}\mathbf{0}\\ k\end{pmatrix}}\right)_0\right],\end{aligned} \tag{5}$$

where $r_{ij} = |\mathbf{r}_{ij}|$. Eq. (5) expresses the force constants of the phonon vibration by six derivatives of the potential (one should notice that for $k = l$ and $k \neq l$, $\left(\frac{\partial^2\varphi_1}{\partial\cos\theta_{ijk}\partial\cos\theta_{ijl}}\right)_0$ correspond to two different derivatives). The last five of these derivatives are closely related to the macroscopic mechanical constants of grapheme [30].

For the second order derivative of the long-range interactions in graphene, an expansion similar to Eq. (5) can be obtained as

$$\begin{aligned}\left(\frac{\partial^2\varphi_m(\mathbf{r}_{ij})}{\partial u_\alpha\begin{pmatrix}\mathbf{0}\\ k\end{pmatrix}\partial u_\beta\begin{pmatrix}\mathbf{l}'\\ k'\end{pmatrix}}\right)_0 &= \left(\frac{\partial\varphi_m}{\partial r_{ij}}\right)_0\left(\frac{\partial^2 r_{ij}}{\partial u_\alpha\begin{pmatrix}\mathbf{0}\\ k\end{pmatrix}\partial u_\beta\begin{pmatrix}\mathbf{l}'\\ k'\end{pmatrix}}\right)_0\\ &+\left(\frac{\partial^2\varphi_m}{\partial r_{ij}^2}\right)_0\left(\frac{\partial r_{ij}}{\partial u_\alpha\begin{pmatrix}\mathbf{0}\\ k\end{pmatrix}}\frac{\partial r_{ij}}{\partial u_\beta\begin{pmatrix}\mathbf{l}'\\ k'\end{pmatrix}}\right)_0,\end{aligned} \tag{6}$$

where $m = 2, 3$. The expansions in Eq. (5) and Eq. (6) are useful for analyzing the phonon spectrum and related physical properties. For graphene, we find that the first terms on the RHS of Eq. (5) and Eq. (6) with the form $\left(\frac{\partial\varphi_k}{\partial r_{ij}}\right)_0\left(\frac{\partial^2 r_{ij}}{\partial u_\alpha\begin{pmatrix}0\\ k\end{pmatrix}\partial u_\beta\begin{pmatrix}\mathbf{l}'\\ k'\end{pmatrix}}\right)_0$, $(k = 1, 2, 3)$ (hereafter called the FOD terms) has a considerable effect on the phonon spectrum and are crucial for the NTE of graphene in low temperature range. Notice that the ground state lattice constant a_0 (here we mean the equilibrium distance between the nearest neighbors) for graphene is determined by $\frac{\partial\Phi_i}{\partial a} = \frac{1}{2}\frac{\partial}{\partial a}\left[\sum_{j,|\mathbf{r}_{ij}|=a}\varphi_1(\mathbf{r}_{ij},\theta_{ijk}) + \sum_{j,|\mathbf{r}_{ij}|=\sqrt{3}a}\varphi_2(\mathbf{r}_{ij}) + \sum_{j,|\mathbf{r}_{ij}|=2a}\varphi_3(\mathbf{r}_{ij})\right] = 0$, where a is the nearest neighbor distance in graphene. To make the sum of this three terms zero, $\left(\frac{\partial\varphi_k}{\partial a}\right)_0$, $(k = 1, 2, 3)$ are all nonzero quantities even at ground state, which leads to nonvanishing FOD

terms. This result can no longer hold if only nearest neighbor interaction is considered.

From its definition, the linear thermal expansion coefficients are given by $\alpha_k = \frac{1}{a_k}\frac{\partial a_k}{\partial T}$, where summation rule is not applied and $a_k (k = 1, 2)$ denotes the characteristic length of the lattice cell in x-axis and y-axis. Following the Grüneisen formalism [31], we have alternatively

$$\alpha_k = \sum_{\mathbf{q},n} c_v(\mathbf{q}, n) \sum_i \frac{s_{ik}}{S_0} \gamma_i(\mathbf{q}, n), \tag{7}$$

where s_{ik} is the in-plane elastic compliance matrix and S_0 is the equilibrium area of the primitive cell. $c_v(\mathbf{q}, n)$ denotes the contribution to the specific heat from the mode $(\mathbf{q}, n)$

$$c_v(\mathbf{q}, n) = k_B \left(\frac{\hbar\omega_{\mathbf{q}n}}{2k_B T}\right)^2 \frac{1}{\sinh^2\left(\frac{\hbar\omega_{\mathbf{q}n}}{2k_B T}\right)}, \tag{8}$$

and $\gamma_i(\mathbf{q}, n)$ is called the Grüneisen parameter for mode $(\mathbf{q}, n)$.

$$\gamma_i(\mathbf{q}, n) = \frac{-a_{0,i}}{\omega_{0,\mathbf{q}\lambda}} \left(\frac{\partial\omega_{\mathbf{q}n}}{\partial a_i}\right)_0. \tag{9}$$

In Fig. 1, based on the potential LCBOPII, we plot $\gamma_i(\mathbf{q}, n)$ for all the phonon modes for graphene (with red lines). Here we take $\gamma_i(\mathbf{q}, n) = \frac{-a}{2\omega_{0,\mathbf{q}\lambda}} \left(\frac{\partial\omega_{\mathbf{q}n}}{\partial a}\right)_0$. The overall structure of the spectrum of $\gamma_i(\mathbf{q}, n)$ in Fig. 1 (plotted with red lines) is quite similar to the one obtained in Ref. [25] using a different carbon–carbon interaction potential, especially for the in-plane branches. For the ZA modes, large negative Grüneisen parameters are found in both our calculation and Mounet and Marzari's work. However, the lowest Grüneisen parameter obtained in Ref. [25] next to the Γ point (i.e., at long wavelength limit) is −80, while the lowest Grüneisen parameter obtained in our work approaches $-\infty$. To understand this singularity of Grüneisen parameter, we solve the ZA mode at long wavelength limit for graphene as

$$\omega_{\mathbf{ZA}}^2 = b_2 q^2 + b_4 q^4, \tag{10}$$

where $q = |\mathbf{q}|$ and

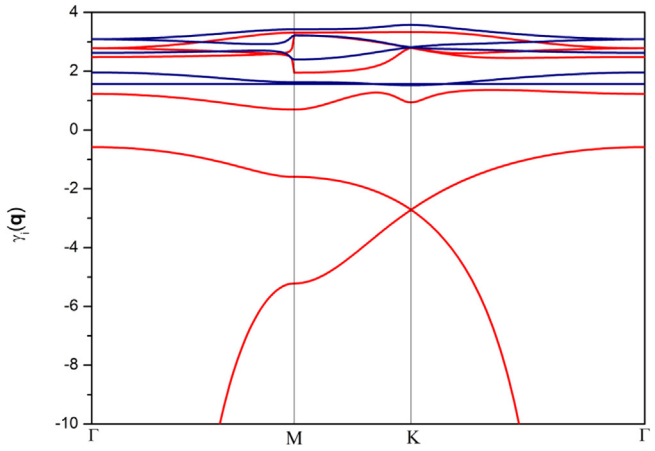

Fig. 1. Mode Grüneisen parameters for graphene, red lines plotted with the FOD terms, blue lines plotted without the FOD terms. (A colour version of this figure can be viewed online.)

$$\begin{aligned} b_2 &= \frac{3}{4m} a \frac{\partial}{\partial a}[\varphi_1 + 2\varphi_2 + \varphi_3], \\ b_4 &= \frac{3}{64m} a^2 \left\{ 24 \frac{\partial\varphi_1}{\partial\cos\theta_{ijk}} - a\frac{\partial}{\partial a}[\varphi_1 + 6\varphi_2 + 4\varphi_3] \right\}. \end{aligned} \tag{11}$$

Since every carbon atom in graphene has three nearest neighbors, six second nearest neighbors and three third nearest neighbors, b_2 in Eq. (11) can be rewritten as $b_2 = \frac{a}{2m}\frac{\partial\Phi_i}{\partial a}$. We have at ground state $\left(\frac{\partial\Phi_i}{\partial a}\right)_0 = 0$ (neglecting the effect of zero point vibration), and at absolute zero Eq. (10) is reduced to

$$\omega_{0,\mathbf{ZA}} = \sqrt{(b_4)_0} q^2, \tag{12}$$

where $\omega_{0,\mathbf{ZA}}$ denotes the frequency of the ZA mode at long wavelength limit at ground state. For graphene at long wavelength limit, the Grüneisen parameters for the ZA modes are obtained as

$$\gamma_{ZA}(\mathbf{q}) = \frac{-a}{4(b_4)_0 q^4} \left[\left(\frac{\partial b_2}{\partial a}\right)_0 q^2 + \left(\frac{\partial b_4}{\partial a}\right)_0 q^4 \right]. \tag{13}$$

Although $(b_2)_0$ vanishes at ground state, $(\frac{\partial b_2}{\partial a})_0 = \frac{a}{2m}(\frac{\partial^2\Phi_i}{\partial a^2})_0$ is positive for a stable lattice structure. Hence we have immediately $\lim_{q\to 0} \gamma_{ZA}(\mathbf{q}) = \frac{-a}{4(b_4)_0 q^2}(\frac{\partial b_2}{\partial a})_0 = -\infty$, where the singularity is caused by consideration of the FOD terms in Eq. (6). In Mounet and Marzari's work [25] this singularity is missing probably because the atomic potential fitted from the first principal calculation is not a multibody potential (i.e., not related to $cos\theta_{ijk}$). The Grüneisen parameters calculated when we neglect the FOD terms is plotted with blue lines in Fig. 1, where we can see that in this case all modes have positive Grüneisen parameters. So the effect of the FOD terms is the only reason for the negative Grüneisen parameters in graphene at ground state. In the low temperature range, the contribution from the ZA modes at long wavelength limit to the thermal expansion coefficient dominates, which implies large NTE coefficient for graphene. This explains the sharp decrease of lattice constant immediately above 0 K in the Monte Carlo simulation of finite temperature lattice properties of graphene [32]. One should notice that the property of the atomic potential is not used in the discussion of $\gamma_{ZA}(\mathbf{q})$, which means NTE coefficient is an intrinsic property for any 2D materials with honeycomb structures in low temperature range. In Appendix A, we further prove that for any monatomic 2D crystals, the dispersion relation for the out-of-plane vibration takes the same form as Eq. (10), with $b_2 = \frac{a}{2m}\frac{\partial\Phi_i}{\partial a}$. According to the discussion given above, NTE is also intrinsic for any monatomic 2D crystals.

We have proved that NTE coefficient is intrinsic for graphene in the low temperature range. The next question is does this NTE coefficient necessarily leads to a rippled state. To answer this question, we assume that at any given temperature T above the zero point, graphene remains in a flat state. In this case, the dispersion relation of the ZA mode at long wavelength limit is still given by Eq. (10) and Eq. (11), where b_2 and b_4 are now calculated at the new equilibrium lattice constant (ELC) a_T instead of a_0. Due to the NTE of graphene in the low temperature range, $a_T < a_0$ and thus $b_2 < 0$. In this case, for small enough q the first term in Eq. (10) dominates and softening of the ZA modes at long wavelength limit is expected, which causes periodic ripples. To be more specific, Eq. (10) can be rewritten as

$$\omega_{\mathbf{ZA}}^2 = b_4 \left(q^2 + \frac{b_2}{2b_4}\right)^2 - \frac{b_2^2}{4b_4}. \tag{14}$$

From Eq. (14), we can see when $b_2 < 0$ (i.e. $a_T < a_0$), all the ZA modes in the interval $q^2 \in \left(0, \left|\frac{b_2}{b_4}\right|\right)$ are softened while the most softened mode is determined by $q^2 = \left|\frac{b_2}{2b_4}\right|$. To illustrate this effect, we plot in Fig. 2 the phonon spectrum of flat graphene at its ground state lattice constant $a = 1.42059\text{Å}$, and at a smaller lattice constant $a = 1.41\text{Å}$. The phonon frequencies in Fig. 2 are obtained in such a way that imaginary frequencies (softened modes) are replaced by corresponding negative frequencies. It is shown in Fig. 2 that for $a = 1.41\text{Å}$, the ZA modes at long wavelength limit are softened. In previous theories for the "bending" waves in strongly anisotropic crystals [27], or the theory of membranes [33], dispersion relation with the form of Eq. (12) is directly used based on elastic theory of thin plates, for which the existence of soft ZA modes cannot be discovered. This explains why the soft modes mechanism of ripples is not seen in these two or other related theoretical works. On the other hand, We notice that by using the quantum field theory, a similar condensation of ZA modes near long wavelength limit is predicted when compressive stress is applied [34]. The physical mechanism of this "buckling transition" is attributed to the interaction between flexural phonons when corrected by the exchange of electron-hole excitation. Since for our analysis, the effect of electron is incorporated in the empirical carbon potential, San-Jose's work may provide an explanation for the soft ZA modes in a subatomic level.

For any ZA mode with wave vector $\mathbf{q}$, the related atomic displacements can be written as $u_{\alpha\mathbf{q}}\begin{pmatrix}\mathbf{l}\\ k\end{pmatrix} = \delta_{\alpha 3} A_{\mathbf{q}} e^{i[\omega_{\mathbf{q}} t - \mathbf{q}(\mathbf{l}_k + \mathbf{R}_k)]}$, where $A_{\mathbf{q}}$ denotes the amplitude and $\mathbf{R}_k$ the relative position vector of the kth atom in the $\mathbf{l}$ th unit cell. When $\omega_{\mathbf{q}} \to 0$, the mode gradually loses its restoring force and ripples with period determined by $\mathbf{q}$ are formed by the out-of-plane displacements $u_{\alpha\mathbf{q}}\begin{pmatrix}\mathbf{l}\\ k\end{pmatrix}$. According to our deduction for flat graphene, all the ZA modes in the interval $q^2 \in (0, \left|\frac{b_2}{b_4}\right|)$ are softened when $b_2 < 0$, which means that starting from a flat configuration, ripples with period larger than $2\pi\sqrt{-\frac{b_4}{b_2}}$ will spontaneously appear. Another vital question is the role of the most softened mode $q^2 = \left|\frac{b_2}{2b_4}\right|$ in ripple formulation. According to the theory of soft modes [35,36], for any existing soft mode with wave vector $\mathbf{q}$, the related free energy can be written as

$$\Delta F = \frac{1}{2}\omega_{\mathbf{q}}^2 Q_{\mathbf{q}}^2 + O\left(Q_{\mathbf{q}}^2\right) + non - critical\ terms, \tag{15}$$

where $Q_{\mathbf{q}}$ denotes the mean value of the normal coordinate of mode $\mathbf{q}$ and $O(Q_{\mathbf{q}}^2)$ denotes higher order terms in $Q_{\mathbf{q}}$. Eq. (15) is valid only when $Q_{\mathbf{q}}$ is small enough, i.e., ΔF is the change of free energy when the system is disturbed from flat configuration. In the harmonic approximation, the mode−mode interaction is neglected, thus the analysis for soft modes with different $\mathbf{q}$ can be done independently. When $\omega_{\mathbf{q}}^2 < 0$, we have from Eq. (15) $Q_{\mathbf{q}} = 0$ corresponds to a non-equilibrium state. Choosing $Q_{\mathbf{q}}$ as the order parameter of the system, the evolution of the system can be studied with the help of thermodynamics of irreversible processes [37,38].

$$\frac{dQ_{\mathbf{q}}}{dt} = -\Gamma\frac{\partial \Delta F}{\partial Q_{\mathbf{q}}} = -\Gamma\omega_{\mathbf{q}}^2 Q_{\mathbf{q}} + O(Q_{\mathbf{q}}), \tag{16}$$

where $\Gamma > 0$ denotes the phenomenological kinetic coefficient. We see from Eq. (16) that for $\omega_{\mathbf{q}}^2 < 0$, $Q_{\mathbf{q}}$ increases with a speed $\frac{dQ_{\mathbf{q}}}{dt}$ that varies linearly with $\left|\omega_{\mathbf{q}}^2\right|$. Therefore, the most softened mode $q^2 = \left|\frac{b_2}{2b_4}\right|$ corresponds to the ripple which evolves with the fastest speed when the initial state of graphene is flat. In this sence, we should expect existence of ripples with many different $\mathbf{q}$ satisfying $q^2 \in \left(0, \left|\frac{b_2}{b_4}\right|\right)$, while the most observable one is with a periodicity determined by $q^2 = \left|\frac{b_2}{2b_4}\right|$.

For material sample with infinite size, the phonon spectrum is continuous for q and the wavelength λ of the ripple that corresponds to the most softened mode at given shrunken ELC can be predicted by Eq. (14)

$$q_s = \sqrt{-\frac{b_2}{2b_4}}, \qquad \lambda = \frac{2\pi}{q_s}. \tag{17}$$

This wavelength λ corresponds to the most observable ripple and thus we call it the *characteristic wavelength* of the ripples. This soft mode-induced mechanism for ripple formation is prior to the fluctuation-induced mechanism [18,19] for two reasons. Firstly, appearance of soft ZA modes depends merely on a shortened lattice constant and it can be derived through lattice dynamics neglecting any anharmonic terms or effect of fluctuation. Secondly, the ripples formed by soft modes refer to a change of the **static equilibrium configuration of graphene,** which reflects the need of the system to evolve to an equilibrium state. In this sense, these ripples are "definite" compared with the fluctuation induced ripples which are more "random". As a result, in the process of soft modes stabilization, the static equilibrium configuration of graphene is no longer flat, which changes the phonon spectrum. Thus the formula given in Eq. (17) should be regarded as a rough estimation of the characteristic ripple size. For a precise calculation of the associated ripple size and thermodynamic properties of graphene, the interplay between the rippling morphology and the phonons should be incorporated. We treat this problem in a subsequent work [39].

For material sample with finite size L^2, discrete phonon spectrum is obtained by using the periodic boundary condition. In this

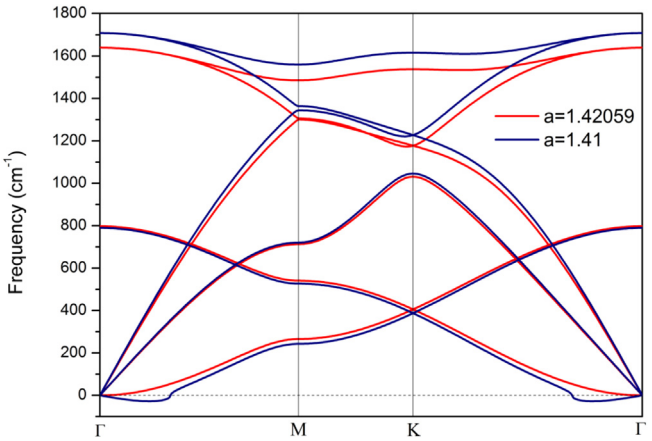

Fig. 2. Phonon Spectrum for graphene, red lines plotted at lattice constant a = 1.42059, blue lines plotted at lattice constant a = 1.41. The modes with negative frequencies are softened. (A colour version of this figure can be viewed online.)

case, the smallest q attainable is related to the sample size by $2\pi/L$. Thus for graphene samples with very small size, it is possible that even the smallest q is outside the interval $\left(0, \left|\frac{b_2}{b_4}\right|\right)$. In this case the graphene sample will maintain flat at low temperature. Of course one should notice that our discussion is restricted by the periodic boundary condition. For any real material sample with finite size, the actual boundary condition will change the vibrational modes of the sample and therefore has significant influence in the stability and ripple size. This is an interesting topic which requires further analysis.

The variation of the characteristic wavelength λ of the ripples with ELC predicted by Eq. (17) is plotted in Fig. 3(a), from which we observe a drop of λ when the ELC decreases from its ground state value. By Monte Carlo simulation, the finite temperature ELC of graphene is calculated [32] for a sample of 8640 atoms, and ripples with wavelength of about 80 Å is found at 300 K [18]. We extract the finite temperature ELC in Zakharchenko et al.'s work [32] and calculated the characteristic wavelength λ of the soft-mode induced ripples from Eq. (17). The results are plotted in Fig. 3(b). An "U" shaped curve with $\lambda > 40$ Å is obtained for the variation of λ with temperature, and at 300 K λ is evaluated to be 42 Å using Eq. (17). This result is compatible with experimental findings [1] (50–100 Å).

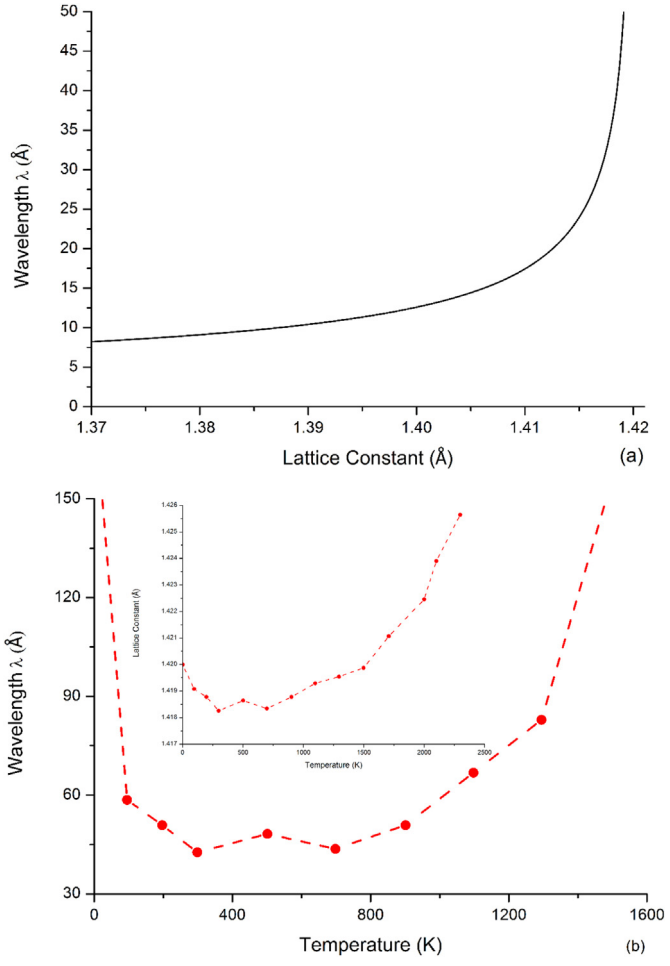

Fig. 3. Variation of the characteristic wavelength of ripples in graphene with (a) lattice constant and (b) temperature. The inset in (b) shows the variation of lattice constant with temperature, extracted from Fig. 1 in Zakharchenko et al.'s work [32]. (A colour version of this figure can be viewed online.)

3. Finite-temperature analysis

According to the above discussion, a flat graphene at ground state is crumpled as temperature raises, owing to the decreased ELC caused by the intrinsic NTE coefficient. Yet this intrinsic NTE coefficient is obtained based on the flat configuration of graphene, which is only true at ground state. At finite temperature, graphene stabilizes itself in a rippled state which tends to eliminate the large negative Grüneisen parameters corresponding to the ZA modes at long wavelength limit. On the other hand, it is well known that the low lying ZA modes for low-dimensional materials lead to significant out-of-plane fluctuation [27] which is crucial for understanding their thermodynamic properties. To analyze the relation between thermal fluctuation and the NTE coefficient of graphene at finite temperature, we approximate the phonon calculation by neglecting the FOD terms in Eq. (6). One should notice that this approximation is equivalent to a replacement of Eq. (10) by Eq. (12) in terms of the dispersion relation of the ZA modes. It is already known from the blue curves in Fig. 1 that by taking this approximation, the Grüneisen parameters for all modes are positive at ground state.

Based on the approximated phonon calculation, we calculate the ELC of graphene at different temperature points with two models, the quasi-harmonic approximation (QH) and the self-consistent harmonic approximation (SCH), and plot the results in Fig. 4.

Within the QH approximation, the effect of thermal fluctuation is completely neglected. On the other hand, the SCH model derives from the self-consistent phonon (SCP) theory [40–42], which treats the situation in lattice dynamics where the amplitude of atomic vibration can no longer considered negligible so that anharmonic effects have to be taken into account. The Helmholtz free energy within the SCH takes the following form

$$F_{SCH} = \frac{1}{2}\sum_{\substack{i,j \\ i\neq j}} \left\langle \Phi\left(\mathbf{r}_{ij}, \theta_{ijk}\right)\right\rangle_0 + k_B T \sum_{\mathbf{q},\lambda} \ln\left[2\sinh\left(\frac{\hbar\omega_{\mathbf{q}\lambda}}{2k_B T}\right)\right] - \frac{1}{4}\sum_{\mathbf{q},\lambda} \hbar\omega_{\mathbf{q}\lambda} \coth\frac{\hbar\omega_{\mathbf{q}\lambda}}{2k_B T}, \tag{18}$$

where $\langle\ldots\rangle_0$ denotes statistical average over the states described by the Hamiltonian of the system under harmonic interactions

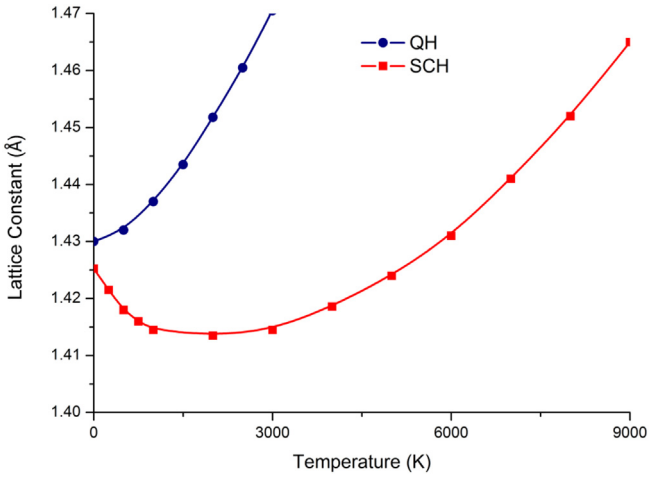

Fig. 4. Temperature dependence of the lattice constant predicted by the SCH (red line) and QH (blue line). (A colour version of this figure can be viewed online.)

$$H_0 = \frac{1}{2}\sum_{\substack{i,j\\ i\neq j}} \Phi(\mathbf{R}_{ij}) + \frac{1}{2}\sum_{\substack{i,j\\ i\neq j}} \frac{1}{2}\mathbf{u}^T(i,j)\mathbf{K}(i,j)\mathbf{u}(i,j) + \sum_i \frac{|\mathbf{P}_i|^2}{2m}, \tag{19}$$

To be more specific, the first term on the RHS of Eq. (18) is most conveniently evaluated by using the following formula

$$\left\langle \Phi\left(\mathbf{r}_{ij},\theta_{ijk}\right)\right\rangle_0 = \left[(2\pi)^3 \det\mathbf{\Lambda}(i,j)\right]^{-\frac{1}{2}} \int d^3u \Phi(\mathbf{R}_{ij}+\mathbf{u}) \exp\left[-\frac{1}{2}u_\alpha \Lambda^{-1}_{\alpha\beta}(i,j)u_\beta\right], \tag{20}$$

where $\Lambda^{-1}_{\alpha\beta}(i,j)$ denote components of the inverse matrix of $\mathbf{\Lambda}(i,j)$, with components

$$\Lambda_{\alpha\beta}\begin{pmatrix}\mathbf{0},\mathbf{l}'\\ kk'\end{pmatrix} = \left\langle\left[u_\alpha\begin{pmatrix}\mathbf{0}\\ k\end{pmatrix} - u_\beta\begin{pmatrix}\mathbf{l}'\\ k'\end{pmatrix}\right]^2\right\rangle_0 = \frac{\hbar}{mN}\sum_{\mathbf{q},n,k,k'} \varepsilon_{\alpha k}(\mathbf{q},n)\varepsilon_{\beta k'}(\mathbf{q},n)\left[e^{i\mathbf{q}\mathbf{R}_{0k}} - e^{i\mathbf{q}\mathbf{R}_{l'k'}}\right]\omega^{-1}_{\mathbf{q}n}\coth\frac{\hbar\omega_{\mathbf{q}n}}{2k_BT}. \tag{21}$$

From Fig. 4, we find that NTE presents itself in the curve obtained within the SCH up to about 2000 K, but not in the curve obtained within the QH. Comparing the blue curve (QH) with Fig. 12 in Ref. [25] which also plots the variation of ELC with temperature calculated within QH, we can see that the trend of their curve is opposite to ours. This discrepancy is due to the fact that our calculation is based on an approximated phonon spectrum which neglects the FOD terms in Eq. (6). In this case the Grüneisen parameters for all modes are positive at ground state according to Fig. 1 and positive thermal expansion is expected. In other words, the NTE presented in Fig. 12 in Ref. [25] is induced by the FOD terms only. Yet by comparing the red curve and blue curve in Fig. 4, we see that NTE still exists in the result of SCH model when the effect of FOD terms are excluded. This means that besides the FOD terms, the large out-of-plane fluctuation provides another origin for the NTE coefficient of graphene at finite temperature. Moreover, anharmonic effects caused mainly by ZA modes can be significant even at low temperature since the slope of the red curve in Fig. 4 is changed compared with that of the blue curve immediately above 0 K. The shape of the red curve in Fig. 4 is very similar to the curve of lattice constants with temperature obtained in Zakharchenko et al.'s work [32], except that the temperature scale in Fig. 4 is larger. The temperature scale difference between Fig. 4 and Zakharchenko's work can be explained by the omission of third order terms in the expansion of atomic potentials in the SCH model. Inclusion of third order terms leads to phonon–phonon interaction which lowers the mode frequencies and finally results in larger ELC at given temperature.

To explain physically why large out-of-plane fluctuation is causing NTE, we first come to the equation which determines the ELC

$$\left[\frac{\partial F(T,R_{ij})}{\partial R_{ij}}\right]_T = 0, \tag{22}$$

where the free energy of the system takes different expressions in different models. Generally, we have

$$F = F_\Phi + F_\mathrm{v}, \tag{23}$$

where F_Φ denotes contribution from the atomistic potential, and F_v denotes contribution from the phonon vibration to the free energy. Substituting Eq. (23) into Eq. (22), we have

$$P_\Phi - P_\mathrm{v} = 0, \tag{24}$$

where

$$P_\Phi = -\frac{1}{N}\left[\frac{\partial F_\Phi}{\partial R_{ij}}\right]_T, \quad P_\mathrm{v} = \frac{1}{N}\left[\frac{\partial F_\mathrm{v}}{\partial R_{ij}}\right]_T. \tag{25}$$

In Eq. (25) N denotes the number of atoms in the system. P_Φ and P_v can be understood as the averaged "force" acted on each atom in the system due to atomistic interaction and phonon vibration. For the two models QH and SCH, the expressions of F_Φ and F_v are given by

$$F_{\Phi,QH} = \frac{1}{2}\sum_{\substack{i,j\\ i\neq j}} \Phi\left(\mathbf{r}_{ij},\theta_{ijk}\right), F_{\mathrm{v},QH} = k_BT\sum_{\mathbf{q},n}\ln\left[2\sinh\left(\frac{\hbar\omega_{\mathbf{q}n}}{2k_BT}\right)\right]. \tag{26}$$

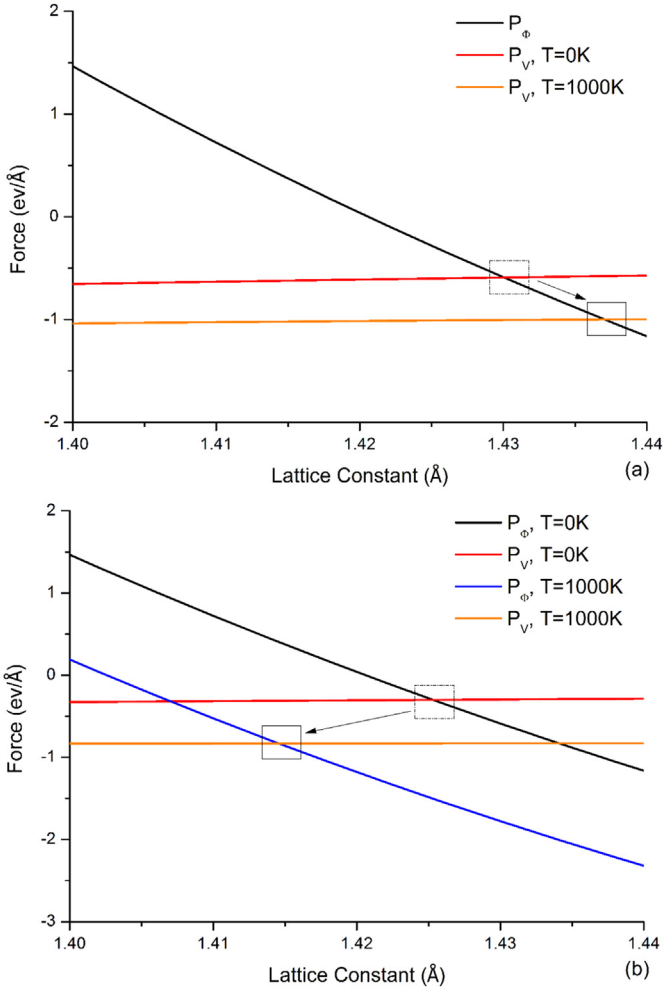

Fig. 5. Variation of $\boldsymbol{P}_\Phi$ and $\boldsymbol{P}_\mathrm{v}$ with lattice constant at $T = 0$ K and $T = 1000$ K using (a) QH and (b) SCH. The dotted boxes marked the equilibrium points and the arrows indicate the variation tendency of lattice constant due to the temperature change. (A colour version of this figure can be viewed online.)

$$F_{\Phi,\,SCH} = \frac{1}{2}\sum_{\substack{i,j\\ i\neq j}}\left\langle \Phi\left(\mathbf{r}_{ij},\theta_{ijk}\right)\right\rangle_0,$$

$$F_{v,SCH} = k_BT\sum_{\mathbf{q},n}\ln\left[2\sinh\left(\frac{\hbar\omega_{\mathbf{q}n}}{2k_BT}\right)\right] - \frac{1}{4}\sum_{\mathbf{q},n}\hbar\omega_{\mathbf{q}n}\coth\frac{\hbar\omega_{\mathbf{q}n}}{2k_BT}. \tag{27}$$

In Fig. 5 we plot the variation of P_Φ and P_v with lattice constant at $T = 0$ K and $T = 1000$ K using the two models. From Eq. (26) we see that within the QH, F_Φ and thus P_Φ are independent of temperature, which means that the variation of ELC with temperature is governed by change of F_v and thus P_v. In Fig. 5(a), the curve for P_v is down-shifted when T increases from 0 K to 1000 K, resulting in an increase of the ELC and thus a positive thermal expansion coefficient. On the other hand, for SCH F_Φ is defined as the ensemble average of the atomistic potential, or called the "smeared potential" [41]. In Eq. (20), the atomic displacement is regarded as a stochastic variable satisfying Gauss distribution with variance $\Lambda_{\alpha\beta}(i,j)$. The consequence is that the interatomic distances are effectively increased, which is termed "vibrational elongation" [43]. For example, the bond length for two neighboring atoms undergoing transverse vibration is always larger than its static value. Actually, this example implies that for low-dimensional materials the effect of vibrational elongation should be more significant than for 3D materials due to large amplitude out-of-plane vibration. This effect is illustrated by the left-shifted P_Φ curve when T changes from 0 K to 1000 K in Fig. 5(b). For the SCH model, the determination of ELC at given temperature is a result of competition between the down-shifting of P_v and left-shifting of P_Φ. When the left-shifting of P_Φ prevails, a drop of ELC is expected, as is shown in Fig. 5(b) when T increases from 0 K to 1000 K. When the temperature further raises, the down-shifting of P_v becomes more significant, which leads to an increase of thermal expansion coefficient and at certain temperature point a positive thermal expansion coefficient is expected.

The effect of FOD terms and the thermal fluctuation are analyzed independently in Sections 2 and 3, both deduced upon flat configuration of graphene. A vital question to ask next is how is the NTE and thermal properties changed when graphene is already stabilized in a rippled state. The answer of this question is not only significant for understanding the actual behavior of graphene in experiments, but also of general interest for studying the structural properties of any membrane-like material. This question is discussed in one of our subsequent works [39].

4. Conclusion

In summary, we elucidate that at low temperature the ripples and the NTE coefficient are two related intrinsic characters for any 2D materials with a honeycomb structure (or any monoatomic 2D crystals). Appearance of soft ZA modes near long wavelength limit for system with shortened ELC is found to be another origin for the ripple formation in graphene besides thermal ZA mode fluctuation. The soft ZA modes and NTE are both caused by the FOD terms in lattice dynamical analysis. The characteristic wavelength of the soft-mode induced ripples is related to the shrunken ELC by Eq. (15). At finite temperature, NTE can be explained by the "vibrational elongation" effect due to large out-of-plane fluctuation, and it should be expected for any 2D materials. Currently, silicene, BN, graphane, MnO_2, etc., are among the possible candidates which have been intensively investigated [44–47] as successors of graphene. Our findings pave the road to the establishment of a soft-mode based thermodynamic theory which is of significance concerning the stability and structure for all 2D materials [39]. They also provide the theoretical foundation for "ripple engineering" of graphene and other 2D materials to tune their electronic, mechanical and other properties. For the next step, it is very interesting and instructive to explore the possible effect of various mechanical loads and boundary conditions on the stability and structure of graphene and other 2D materials.

Acknowledgment

The work was supported by the NSFC (National Natural Science Foundation of China) through the funds (11232015 and 11472313), and the Research Fund for the Doctoral Program of Higher Education of China (20130171130003).

Appendix A. Out-of-plane dispersion relation for monatomic 2D crystals at long wavelength limit

The aim of this appendix is to prove that the out-of-plane dispersion relation for monatomic 2D crystals at long wavelength limit takes the same form as Eq. (10), where the coefficient of the q^2 term is $\frac{a}{2m}\left(\frac{\partial\Phi_i}{\partial a}\right)_0$.

For monatomic crystals, Eqs. (1)–(3) still hold, only with the subscript k, k' abandoned. Here we rewrite the expression for the force constants as

$$K_{\alpha\beta}(\mathbf{0},\mathbf{l}') = \left(\frac{\partial^2 U}{\partial u_\alpha(\mathbf{0})\partial u_\beta(\mathbf{l}')}\right)_0, \tag{A.1}$$

where $U = \sum\Phi_i$ and Φ_i is the potential energy possessed by the ith atom. As the crystal has rotation symmetry, we suppose the monatomic crystal possesses N fold symmetry. Namely, one atom has N nth nearest neighbor atoms. In this case, Φ_i takes the following form

$$\Phi_i = \frac{N}{2}\left[\varphi_1\left(\mathbf{r}_{ij},\theta_{ijk}\right) + \varphi_2\left(\mathbf{r}_{ij}\right) + \ldots\varphi_n\left(\mathbf{r}_{ij}\right)\right], \tag{A.2}$$

where $\varphi_k(\mathbf{r}_{ij})$ denotes the kth nearest neighbor interaction and N denotes the number of nearest neighboring atoms. Here, the nearest neighbor interaction is considered as short range interaction, and the others are considered as long range interaction. The second order derivative of U in Eq. (A.1) can be expanded as

$$\begin{aligned}\left(\frac{\partial^2 U}{\partial u_\alpha(\mathbf{0})\partial u_\beta(\mathbf{l}')}\right)_0 &= \left(\frac{\partial U}{\partial r_{ij}}\right)_0\left(\frac{\partial^2 r_{ij}}{\partial u_\alpha(\mathbf{0})\partial u_\beta(\mathbf{l}')}\right)_0\\ &+\sum_{k\neq i,j}\left(\frac{\partial U}{\partial\cos\theta_{ijk}}\right)_0\left(\frac{\partial^2\cos\theta_{ijk}}{\partial u_\alpha(\mathbf{0})\partial u_\beta(\mathbf{l}')}\right)_0\\ &+\left(\frac{\partial^2 U}{\partial r_{ij}^2}\right)_0\left(\frac{\partial r_{ij}}{\partial u_\alpha(\mathbf{0})}\frac{\partial r_{ij}}{\partial u_\beta(\mathbf{l}')}\right)_0\\ &+\sum_{k,l\neq i,j}\left(\frac{\partial^2 U}{\partial\cos\theta_{ijk}\partial\cos\theta_{ijl}}\right)_0\left(\frac{\partial\cos\theta_{ijk}}{\partial u_\alpha(\mathbf{0})}\frac{\partial\cos\theta_{ijl}}{\partial u_\beta(\mathbf{l}')}\right)_0\\ &+\sum_{k\neq i,j}\left(\frac{\partial^2 U}{\partial\cos\theta_{ijk}\partial r_{ij}}\right)_0\left[\left(\frac{\partial r_{ij}}{\partial u_\alpha(\mathbf{0})}\frac{\partial\cos\theta_{ijk}}{\partial u_\beta(\mathbf{l}')}\right)_0\right.\\ &\left.+\left(\frac{\partial r_{ij}}{\partial u_\beta(\mathbf{l}')}\frac{\partial\cos\theta_{ijk}}{\partial u_\alpha(\mathbf{0})}\right)_0\right].\end{aligned} \tag{A.3}$$

Using Eq. (A.2), similar expansion can be obtained for $\varphi_1(\mathbf{r}_{ij},\theta_{ijk})$ and $\varphi_k(\mathbf{r}_{ij})$, $k>1$ in the same way.

For 2D crystals, we have

$$\begin{aligned}\mathbf{r_{ij}} &= [x(\boldsymbol{j}) + u_1(\boldsymbol{j}) - x(\boldsymbol{i}) - u_1(\boldsymbol{i}), y(\boldsymbol{j}) + u_2(\boldsymbol{j}) - y(\boldsymbol{i}) - u_2(\boldsymbol{i}), u_3(\boldsymbol{j}) - u_3(\boldsymbol{i})]^T,\\ \mathbf{r_{ik}} &= [x(\boldsymbol{k}) + u_1(\boldsymbol{k}) - x(\boldsymbol{i}) - u_1(\boldsymbol{i}), y(\boldsymbol{k}) + u_2(\boldsymbol{k}) - y(\boldsymbol{i}) - u_2(\boldsymbol{i}), u_3(\boldsymbol{k}) - u_3(\boldsymbol{i})]^T.\end{aligned} \tag{A.4}$$

and $r_{ij} = |\mathbf{r_{ij}}|$, $cos\theta_{ijk} = \frac{\mathbf{r_{ij}}\cdot\mathbf{r_{ik}}}{|\mathbf{r_{ij}}||\mathbf{r_{ik}}|}$. Therefore we have from Eq. (A.4):

$$\begin{aligned}&\left(\frac{\partial r_{ij}}{\partial u_3(\boldsymbol{i})}\right)_0 = 0, \left(\frac{\partial cos\theta_{ijk}}{\partial u_3(\boldsymbol{i})}\right)_0 = 0, \left(\frac{\partial cos\theta_{ijk}}{\partial u_3(\boldsymbol{j})}\right)_0 = 0, \left(\frac{\partial^2 r_{ij}}{\partial u_3(\boldsymbol{i})\partial u_3(\boldsymbol{j})}\right)_0 = -\frac{1}{|r_{ij}|},\\ &\left(\frac{\partial^2 cos\theta_{ijk}}{\partial u_3(\boldsymbol{i})\partial u_3(\boldsymbol{j})}\right)_0 = -\frac{1}{r_{ij}r_{ik}} + \frac{cos\theta_{ijk}}{r_{ij}^2}, \left(\frac{\partial^2 cos\theta_{ijk}}{\partial u_3(\boldsymbol{j})\partial u_3(\boldsymbol{k})}\right)_0 = \frac{1}{r_{ij}r_{ik}},\\ &\left(\frac{\partial^2 r_{ij}}{\partial u_3(\boldsymbol{i})\partial u_\alpha(\boldsymbol{j})}\right)_0 = 0, \left(\frac{\partial^2 cos\theta_{ijk}}{\partial u_3(\boldsymbol{i})\partial u_\alpha(\boldsymbol{j})}\right)_0 = 0, \left(\frac{\partial^2 cos\theta_{ijk}}{\partial u_3(\boldsymbol{j})\partial u_\alpha(\boldsymbol{k})}\right)_0 = 0,\end{aligned} \tag{A.5}$$

where $\alpha = 1, 2$.

We have from Eq. (A.1) and Eq. (A.5) that $K_{3\alpha}(0,\mathbf{l}') = K_{\alpha 3}(0,\mathbf{l}') = 0$, $\alpha = 1,2$. It means the out-of-plane vibration and in-plane vibration are mutually independence. This result can also be obtained by using group theory. As a result, the dispersion relation for the out-of-plane vibration has the form:

$$\omega_{\mathbf{q}3}^2 = D_{33}(\mathbf{q}), \tag{A.6}$$

where

$$D_{33}(\mathbf{q}) = \frac{1}{m}\sum_{\mathbf{l}'} K_{33}(0,\mathbf{l}')e^{-i\mathbf{q}\mathbf{l}'}. \tag{A.7}$$

For convenience, we rewrite the force constant $K_{33}(0,0)$, the nearest neighbor force constant $K_{33}(0,\boldsymbol{l}_1)$, … and the n th nearest neighbor force constant $K_{33}(0,\boldsymbol{l}_n)$ as $\gamma_0, \gamma_1, \ldots \gamma_n$, respectively. Due to the translational invariance, we have $\gamma_0 = -N(\gamma_1 + \gamma_2 \ldots + \gamma_n)$. Thus we have from Eq. (A.6)

$$\begin{aligned}\omega_{\mathbf{q}3}^2 &= \frac{1}{m}\sum_{\boldsymbol{l}} K_{33}(0,\boldsymbol{l})e^{-i\boldsymbol{k}\cdot\boldsymbol{l}}\\ &= \frac{1}{m}\left\{\gamma_0 + \sum_{n=0}^{N-1}\gamma_1 e^{i\left[k_x * a_1\ cos\left(\frac{2n\pi}{N}+\varphi_1\right) + k_y * a_1\ sin\left(\frac{2n\pi}{N}+\varphi_1\right)\right]} + \ldots + \sum_{n'=0}^{N-1}\gamma_n e^{i\left[k_x * a_n\ cos\left(\frac{2n'\pi}{N}+\varphi_n\right) + k_y * a_n\ sin\left(\frac{2n'\pi}{N}+\varphi_n\right)\right]},\end{aligned} \tag{A.8}$$

where a_1 is the nearest neighbor distance, a_2 is the second nearest neighbor distance and a_n is the n th nearest neighbor distance. At long wavelength limit, we expand Eq. (A.8) and obtain

$$\begin{aligned}\omega_{\mathbf{q}3}^2 = &-\frac{N}{4m}\left(\gamma_1 a_1^2 + \gamma_2 a_2^2 \ldots + \gamma_n a_n^2\right)q^2\\ &+ \frac{N}{64m}\left(\gamma_1 a_1^4 + \gamma_2 a_2^4 \ldots + \gamma_n a_n^2\right)q^4.\end{aligned} \tag{A.9}$$

Because γ_l, ($l = 0, 1, \ldots, n$) is second order derivative of U with respect to $u_3(0)$ and $u_3(\mathbf{l})$, from Eq. (A.3) we learn that the expression of γ_l can be divided into two parts: the FOD terms $(\frac{\partial U}{\partial r_{ij}})_0(\frac{\partial^2 r_{ij}}{\partial u_z(\mathbf{0})\partial u_z(\mathbf{l})})_0$, and the bond angle (BA) terms $\sum_{k\neq i,j}(\frac{\partial U}{\partial cos\ \theta_{ijk}})_0\ (\frac{\partial^2\ cos\ \theta_{ijk}}{\partial u_\alpha(\mathbf{0})\partial u_\beta(\mathbf{l})})_0$. Therefore we have

$$\begin{aligned}-\frac{N}{4m}\left(\gamma_1 a_1^2 + \gamma_2 a_2^2 \ldots + \gamma_n a_n^2\right) = &\left[-\frac{N}{4m}\left(\gamma_1 a_1^2 + \gamma_2 a_2^2 \ldots + \gamma_n a_n^2\right)\right]_{FOD}\\ &+ \left[-\frac{N}{4m}\left(\gamma_1 a_1^2 + \gamma_2 a_2^2 \ldots + \gamma_n a_n^2\right)\right]_{BA},\end{aligned} \tag{A.10}$$

where

$$\begin{aligned}&\left[-\frac{N}{4m}\left(\gamma_1 a_1^2 + \gamma_2 a_2^2 \ldots + \gamma_n a_n^2\right)\right]_{FOD}\\ &= \frac{N}{4m}\left[a\left(\frac{\partial\varphi_1}{\partial a}\right)_0 + a_2\left(\frac{\partial\varphi_2}{\partial a_2}\right)_0 \ldots + a_n\left(\frac{\partial\varphi_n}{\partial a_n}\right)_0\right] = \frac{a}{2m}\left(\frac{\partial\Phi_i}{\partial a}\right)_0.\end{aligned} \tag{A.11}$$

Then we only have to prove that the BA terms in Eq. (A.10) vanish. As mention above, only the nearest neighbor interaction potential possesses bond angle variables. So we just focus on the N angles with atom 0 and atom $\boldsymbol{l}_1$ as their two vertexes. Since $cos\theta_{ijk}=\frac{\mathbf{r}_{ij}\cdot\mathbf{r}_{ik}}{|\mathbf{r}_{ij}||\mathbf{r}_{ik}|}$, we see immediately that the BA terms is related to the motion of multiple neighboring atoms.

$$8\left(\frac{\partial U}{\partial cos\theta_1}\right)_0\left(\frac{\partial^2 cos\theta_1}{\partial u_z(\mathbf{0})\partial u_z(\boldsymbol{l_1})}\right)_0+4\left(\frac{\partial U}{\partial cos\theta_1'}\right)_0\times\left(\frac{\partial^2 cos\theta_1'}{\partial u_z(\mathbf{0})\partial u_z(\boldsymbol{l_1})}\right)_0=0. \tag{A.13}$$

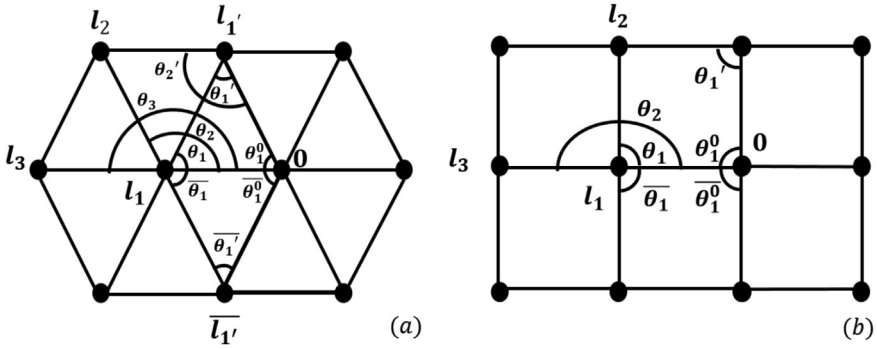

Fig. A1. Two lattice structures of monatomic 2D crystals: triangular lattice (a) and square lattice (b).

For monatomic 2D crystals, only two situations should be considered, which are plotted in Fig. A1. If $\theta_1=\frac{\pi}{3}$, the lattice structure of crystal is triangular lattice (Fig. A1(a)). If $\theta_1=\frac{\pi}{2}$, the lattice structure of crystal is square lattice (Fig. A1(b)). For triangular lattice and square lattice, only the BA terms of γ_1, γ_2, γ_3 are nonzero.

We first deal with the BA terms of the nearest neighbor force constant γ_1. When $\theta_1=\frac{\pi}{3}$, the BA term of γ_1 is affected by $\theta_1,\theta_1^{'},\theta_2,\theta_3$ and their equivalent angles (some of the related angles are shown in Fig. A1(a)). Notice that equivalent angles have equivalent effect on γ_1.For the BA terms of γ_1, due to the geometry of triangular lattice, it is found that three angles (θ_1^0,$\overline{\theta_1}$ and $\overline{\theta_1^0}$) are the equivalent angles of θ_1 and one angle ($\overline{\theta_1'}$) is the equivalent angle of θ_1'. Similarly, θ_2 and θ_3 have three and one equivalent angles, respectively. Thus, the BA term of γ_1 has the form

$$\begin{aligned}[\gamma_1]_{BA}=&8\left(\frac{\partial U}{\partial cos\theta_1}\right)_0\left(\frac{\partial^2 cos\theta_1}{\partial u_z(\mathbf{0})\partial u_z(\boldsymbol{l_1})}\right)_0\\&+8\left(\frac{\partial U}{\partial cos\theta_2}\right)_0\left(\frac{\partial^2 cos\theta_2}{\partial u_z(\mathbf{0})\partial u_z(\boldsymbol{l_1})}\right)_0\\&+4\left(\frac{\partial U}{\partial cos\theta_3}\right)_0\left(\frac{\partial^2 cos\theta_3}{\partial u_z(\mathbf{0})\partial u_z(\boldsymbol{l_1})}\right)_0\\&+4\left(\frac{\partial U}{\partial cos\theta_1'}\right)_0\left(\frac{\partial^2 cos\theta_1'}{\partial u_z(\mathbf{0})\partial u_z(\boldsymbol{l_1})}\right)_0.\end{aligned} \tag{A.12}$$

According to Eq. (A.5), we have

Then Eq. (A.12) can be rewritten as

$$\begin{aligned}[\gamma_1]_{BA}=&8\left(\frac{\partial U}{\partial cos\theta_2}\right)_0\left(\frac{\partial^2 cos\theta_2}{\partial u_z(\mathbf{0})\partial u_z(\boldsymbol{l_1})}\right)_0\\&+4\left(\frac{\partial U}{\partial cos\theta_3}\right)_0\left(\frac{\partial^2 cos\theta_3}{\partial u_z(\mathbf{0})\partial u_z(\boldsymbol{l_1})}\right)_0.\end{aligned} \tag{A.14}$$

The BA term of γ_2 is attributed to θ_2, θ_2'. Since $\theta_2=\theta_2^{'}$, we have

$$[\gamma_2]_{BA}=4\left(\frac{\partial U}{\partial cos\theta_2}\right)_0\left(\frac{\partial^2 cos\theta_2}{\partial u_z(\mathbf{0})\partial u_z(\boldsymbol{l_2})}\right)_0. \tag{A.15}$$

The BA term of γ_3 can be derived in a similar way, where only θ_3 should be considered:

$$[\gamma_3]_{BA}=2\left(\frac{\partial U}{\partial cos\theta_3}\right)_0\left(\frac{\partial^2 cos\theta_3}{\partial u_z(\mathbf{0})\partial u_z(\boldsymbol{l_3})}\right)_0. \tag{A.16}$$

For triangular lattice, using Eq. (A.5), we obtain

$$\begin{aligned}&\left[-\frac{N}{4m}\left(\gamma_1a_1^2+\gamma_2a_2^2\ldots+\gamma_na_n^2\right)\right]_{BA}=-\frac{N}{4m}\left\{[\gamma_1]_{BA}a_1^2+[\gamma_2]_{BA}a_2^2+[\gamma_3]_{BA}a_3^2\right\}\\&=-\frac{N}{4m}\left\{4\left(\frac{\partial U}{\partial cos\theta_2}\right)_0\left[2\left(\frac{\partial^2 cos\theta_2}{\partial u_z(\mathbf{0})\partial u_z(\boldsymbol{l_1})}\right)_0a_1^2+\left(\frac{\partial^2 cos\theta_2}{\partial u_z(\mathbf{0})\partial u_z(\boldsymbol{l_2})}\right)_0a_2^2\right]+2\left(\frac{\partial U}{\partial cos\theta_3}\right)_0\left[2\left(\frac{\partial^2 cos\theta_3}{\partial u_z(\mathbf{0})\partial u_z(\boldsymbol{l_1})}\right)_0a_1^2+\left(\frac{\partial^2 cos\theta_3}{\partial u_z(\mathbf{0})\partial u_z(\boldsymbol{l_3})}\right)_0a_3^2\right]\right\}=0.\end{aligned} \tag{A.17}$$

Thus for triangular lattice, the effect of the BA terms vanishes.

When $\theta_1 = \frac{\pi}{2}$, the BA terms of γ_1 is affected by θ_1, θ_2 and their equivalent angles (some of the related angles are shown in Fig. A1(b)). Similar to the discussion for triangular lattice, θ_1 has three equivalent angles (θ_1^0, $\overline{\theta_1}$ and $\overline{\theta_1^0}$). But θ_2 has one equivalent angles (not shown in Fig. A1(b)). Therefore, we obtain

$$[\gamma_1]_{BA} = 8\left(\frac{\partial U}{\partial cos\theta_1}\right)_0\left(\frac{\partial^2 cos\theta_1}{\partial u_z(\mathbf{0})\partial u_z(\boldsymbol{l_1})}\right)_0 + 4\left(\frac{\partial U}{\partial cos\theta_2}\right)_0\left(\frac{\partial^2 cos\theta_2}{\partial u_z(\mathbf{0})\partial u_z(\boldsymbol{l_1})}\right)_0 \quad (A.18)$$

For the BA terms of γ_2 and γ_3, we have

$$[\gamma_2]_{BA} = 4\left(\frac{\partial U}{\partial cos\theta_1}\right)_0\left(\frac{\partial^2 cos\theta_1}{\partial u_z(\mathbf{0})\partial u_z(\boldsymbol{l_2})}\right)_0, \quad (A.19)$$

$$[\gamma_3]_{BA} = 2\left(\frac{\partial U}{\partial cos\theta_2}\right)_0\left(\frac{\partial^2 cos\theta_2}{\partial u_z(\mathbf{0})\partial u_z(\boldsymbol{l_3})}\right)_0. \quad (A.20)$$

Similar to Eq. (A.17), for square lattice we obtain

$$\left[-\frac{N}{4m}\left(\gamma_1 a_1^2+\gamma_2 a_2^2\ldots+\gamma_n a_n^2\right)\right]_{BA} = -\frac{N}{4m}\left\{[\gamma_1]_{BA}a_1^2+[\gamma_2]_{BA}a_2^2+[\gamma_3]_{BA}a_3^2\right\}$$
$$= -\frac{N}{4m}\left\{4\left(\frac{\partial U}{\partial cos\theta_1}\right)_0\left[2\left(\frac{\partial^2 cos\theta_1}{\partial u_z(\mathbf{0})\partial u_z(\boldsymbol{l_1})}\right)_0 a_1^2+\left(\frac{\partial^2 cos\theta_1}{\partial u_z(\mathbf{0})\partial u_z(\boldsymbol{l_2})}\right)_0 a_2^2\right]+2\left(\frac{\partial U}{\partial cos\theta_3}\right)_0\left[2\left(\frac{\partial^2 cos\theta_2}{\partial u_z(\mathbf{0})\partial u_z(\boldsymbol{l_1})}\right)_0 a_1^2+\left(\frac{\partial^2 cos\theta_2}{\partial u_z(\mathbf{0})\partial u_z(\boldsymbol{l_3})}\right)_0 a_3^2\right]\right\}=0. \quad (A.21)$$

Thus for square lattice, the BA terms also vanish. Therefore, we conclude that the effect of the BA terms on any 2D monatomic crystal vanishes and only the FOD terms remains. So from Eq. (A.11) the coefficient for the q^2 term in the expression of $\omega_{\mathbf{q}3}^2$ can be written as $\frac{a}{2m}\left(\frac{\partial \Phi_i}{\partial a}\right)_0$ at long wavelength limit.

References

[1] J.C. Meyer, A.K. Geim, M.I. Katsnelson, K.S. Novoselov, T.J. Booth, S. Roth, The structure of suspended graphene sheets, Nature 446 (7131) (2007) 60–63.
[2] C.C. Chen, W.Z. Bao, J. Theiss, C. Dames, C.N. Lau, S.B. Cronin, Raman spectroscopy of ripple formation in suspended graphene, Nano Lett. 9 (12) (2009) 4172–4176.
[3] R. Peierls, Quelques propriétés typiques des corps solides. Annales de l'institut Henri Poincaré: Presses Universitaires de France 177–222.
[4] L. Landau, ZhETF 7 819, Phys. Z Sowjet 1937 (11) (1937) 556.
[5] N.D. Mermin, Crystalline order in two dimensions, Phys. Rev. 176 (1) (1968) 250.
[6] N. Tombros, C. Jozsa, M. Popinciuc, H.T. Jonkman, B.J. van Wees, Electronic spin transport and spin precession in single graphene layers at room temperature, Nature 448 (7153) (2007), 571-U4.
[7] K.I. Bolotin, K.J. Sikes, Z. Jiang, M. Klima, G. Fudenberg, J. Hone, et al., Ultrahigh electron mobility in suspended graphene, Solid State Commun. 146 (9–10) (2008) 351–355.
[8] M.I. Katsnelson, A.K. Geim, Electron scattering on microscopic corrugations in graphene, Philos. Trans. Ser. A Math. Phys. Eng. Sci. 366 (1863) (2008) 195–204.
[9] T.O. Wehling, A.V. Balatsky, A.M. Tsvelik, M.I. Katsnelson, A.I. Lichtenstein, Midgap states in corrugated graphene: ab initio calculations and effective field theory, Epl Europhys. Lett. 84 (1) (2008).
[10] D. Huertas-Hernando, F. Guinea, A. Brataas, Spin relaxation times in disordered graphene, Eur. Phys. J. Spec. Top. 148 (2007) 177–181.
[11] F. Simon, F. Muranyi, B. Dora, Theory and model analysis of spin relaxation time in graphene – could it be used for spintronics? Phys. Status Solidi B 248 (11) (2011) 2631–2634.
[12] Y. Okada, W.W. Zhou, D. Walkup, C. Dhital, S.D. Wilson, V. Madhavan, Ripple-modulated electronic structure of a 3D topological insulator, Nat. Commun. 3 (2012).
[13] J. Wakabayashi, T. Sano, Magnetoresistance of rippled graphene in a parallel magnetic field, in: Horiba International Conference: The 19th International Conference on the Application of High Magnetic Fields in Semiconductor Physics and Nanotechnology, 2011, p. 334.
[14] C. Lee, X. Wei, J.W. Kysar, J. Hone, Measurement of the elastic properties and intrinsic strength of monolayer graphene, Science 321 (5887) (2008) 385–388.
[15] J.S. Bunch, A.M. van der Zande, S.S. Verbridge, I.W. Frank, D.M. Tanenbaum, J.M. Parpia, et al., Electromechanical resonators from graphene sheets, Science 315 (5811) (2007) 490–493.
[16] D.W. Boukhvalov, M.I. Katsnelson, Enhancement of chemical activity in corrugated graphene, J. Phys. Chem. C 113 (32) (2009) 14176–14178.
[17] X.Y. Fan, R. Nouchi, K. Tanigaki, Effect of charge puddles and ripples on the chemical reactivity of single layer graphene supported by SiO_2/Si substrate, J. Phys. Chem. C 115 (26) (2011) 12960–12964.
[18] A. Fasolino, J.H. Los, M.I. Katsnelson, Intrinsic ripples in graphene, Nat. Mater. 6 (11) (2007) 858–861.
[19] N. Abedpour, M. Neek-Amal, R. Asgari, F. Shahbazi, N. Nafari, M.R.R. Tabar, Roughness of undoped graphene and its short-range induced gauge field, Phys. Rev. B 76 (19) (2007).
[20] W.Z. Bao, F. Miao, Z. Chen, H. Zhang, W.Y. Jang, C. Dames, et al., Controlled ripple texturing of suspended graphene and ultrathin graphite membranes, Nat. Nanotechnol. 4 (9) (2009) 562–566.
[21] R.C. Thompson-Flagg, M.J.B. Moura, M. Marder, Rippling of graphene, Epl-Europhys Lett. 85 (4) (2009).
[22] D. Yoon, Y.W. Son, H. Cheong, Negative thermal expansion coefficient of graphene measured by Raman spectroscopy, Nano Lett. 11 (8) (2011) 3227–3231.
[23] Y.J. Su, H. Wei, R.G. Gao, Z. Yang, J. Zhang, Z.H. Zhong, et al., Exceptional negative thermal expansion and viscoelastic properties of graphene oxide paper, Carbon 50 (8) (2012) 2804–2809.
[24] J. Zhu, C.M. Andres, J.D. Xu, A. Ramamoorthy, T. Tsotsis, N.A. Kotov, Pseudo-negative thermal expansion and the state of water in graphene oxide layered assemblies, Acs Nano 6 (9) (2012) 8357–8365.
[25] N. Mounet, N. Marzari, First-principles determination of the structural, vibrational and thermodynamic properties of diamond, graphite, and derivatives, Phys. Rev. B 71 (20) (2005).
[26] A.A. Maradudin, E.W. Montroll, G.H. Weiss, I. Ipatova, Theory of Lattice Dynamics in the Harmonic Approximation, Academic Press, New York, 1963.
[27] A.M. Kosevich, Front Matter, Wiley Online Library, 2005.
[28] J.H. Los, L.M. Ghiringhelli, E.J. Meijer, A. Fasolino, Improved long-range reactive bond-order potential for carbon. I. construction, Phys. Rev. B 72 (21) (2005).
[29] M. Arroyo, T. Belytschko, An atomistic-based finite deformation membrane for single layer crystalline films, J. Mech. Phys. Solids 50 (9) (2002) 1941–1977.
[30] Y. Huang, J. Wu, K. Hwang, Thickness of graphene and single-wall carbon nanotubes, Phys. Rev. B 74 (24) (2006).
[31] T.H.K. Barron, J.G. Collins, G.K. White, Thermal expansion of solids at low temperatures, Adv. Phys. 29 (4) (1980) 609–730.
[32] K.V. Zakharchenko, M.I. Katsnelson, A. Fasolino, Finite temperature lattice properties of graphene beyond the quasiharmonic approximation, Phys. Rev. Lett. 102 (4) (2009).
[33] D. Nelson, Statistical Mechanics of Membranes and Surfaces, World Scientific, 2004.
[34] P. San-Jose, J. González, F. Guinea, Electron-induced rippling in graphene, Phys. Rev. Lett. 106 (4) (2011), 045502.
[35] M.E. Lines, A.M. Glass, Principles and Applications of Ferroelectrics and Related Materials, Clarendon Press Oxford, 2001.
[36] R. Blinc, B. Žekš, Soft Modes in Ferroelectrics and Antiferroelectrics, North-Holland Publishing Company, Amsterdam, 1974.
[37] L. Landau, I. Khalatnikov, On the anomalous absorption of sound near a second-order phase transition point. Dokl. Akad. Nauk. SSSR; 469–472.
[38] H. Haken, Synergetics, Springer, 1977.
[39] H.F. Hu, The Nature of "Spontaneous Curvature" in Suspended Graphene, ArXiv:150301177, 2015.

[40] T. Koehler, Theory of the self-consistent harmonic approximation with application to solid neon, Phys. Rev. Lett. 17 (2) (1966) 89–91.
[41] P. Choquard, The Anharmonic Crystal, WA Benjamin, New York, 1967.
[42] N. Werthamer, Self-consistent phonon formulation of anharmonic lattice dynamics, Phys. Rev. B 1 (2) (1970) 572–581.
[43] Y. Ida, Theory of melting based on lattice instability, Phys. Rev. 187 (3) (1969) 951–958.
[44] P. Vogt, P. De Padova, C. Quaresima, J. Avila, E. Frantzeskakis, M.C. Asensio, et al., Silicene: compelling experimental evidence for graphenelike two-dimensional silicon, Phys. Rev. Lett. 108 (15) (2012).
[45] D.C. Elias, R.R. Nair, T.M.G. Mohiuddin, S.V. Morozov, P. Blake, M.P. Halsall, et al., Control of graphene's properties by reversible hydrogenation: evidence for graphane, Science 323 (5914) (2009) 610–613.
[46] C.R. Dean, A.F. Young, I. Meric, C. Lee, L. Wang, S. Sorgenfrei, et al., Boron nitride substrates for high-quality graphene electronics, Nat. Nanotechnol. 5 (10) (2010) 722–726.
[47] O. Lopez-Sanchez, D. Lembke, M. Kayci, A. Radenovic, A. Kis, Ultrasensitive photodetectors based on monolayer MoS_2, Nat. Nanotechnol. 8 (7) (2013) 497–501.